

High RF carrier frequency modulation in silicon resonators by coupling adjacent free-spectral-range modes

Lawrence D. Tzuang,¹ Mohammad Soltani,¹ Yoon Ho Daniel Lee,¹ and Michal Lipson^{1,2,*}

¹School of Electrical and Computer Engineering, Cornell University, Ithaca, New York 14853, USA

²Kavli Institute at Cornell, Cornell University, Ithaca, New York 14853, USA

*Corresponding author: ml292@cornell.edu

Received September 17, 2013; revised February 4, 2014; accepted February 14, 2014;
 posted February 20, 2014 (Doc. ID 197840); published March 19, 2014

We demonstrate the modulation of silicon ring resonators at RF carrier frequencies higher than the resonance linewidth by coupling adjacent free-spectral-range (FSR) resonance modes. In this modulator scheme, the modulation frequency is matched to the FSR frequency. As an example, we demonstrate a 20 GHz modulation in a silicon ring with a resonance linewidth of only 11.7 GHz. We show theoretically that this modulator scheme has lower power consumption compared to a standard silicon ring modulator at high carrier frequencies. These results could enable future on-chip high-frequency analog communication and photonic signal processing on a silicon photonics platform. © 2014 Optical Society of America

OCIS codes: (250.4110) Modulators; (230.5750) Resonators.
<http://dx.doi.org/10.1364/OL.39.001799>

Achieving simultaneous low-power and high-frequency operation of silicon resonator modulators [1–3] is challenging since the modulation frequency is limited by the resonance linewidth [4]. While compactness, low drive voltage, and low electrical power consumption make these resonators attractive, their limited operation frequency hinders their utilization in extremely high-frequency (30–300 GHz) microwave photonic applications such as high-speed analog communication and signal processing [5].

Here we modulate a silicon ring resonator at RF carrier frequencies higher than the resonance linewidth by using electrically induced coupling between adjacent free-spectral-range (FSR) modes [6–8]. Compared with recent works that have shown broadband modulation of silicon resonators [9,10], the FSR coupling (FSRC) approach is an inherently narrow bandwidth [6], and it is therefore applicable for analog systems. Although the FSRC phenomenon has been employed in various contexts and optical materials for modulation or frequency conversion purposes [6,7,11–13], demonstrating this modulator using silicon photonics is critical for enabling high-frequency analog applications that can be readily integrated with CMOS electronics. Here we demonstrate a depletion-type silicon ring modulator [1] that efficiently induces such couplings. We further show that the power consumption of a silicon depletion-type FSRC modulator can be much lower than a standard depletion-type silicon ring modulator at high RF carrier frequencies.

We induce the coupling by introducing a refractive index modulation that matches the frequencies and phases between adjacent resonance modes. The FSRC approach as reported in [6,8,13] utilizes the modulation sidebands generated at the adjacent ring resonances. Here we briefly review the operation of the FSRC modulators. In a standard ring modulator [right of Fig. 1(a)], the generated sidebands are filtered by the resonance linewidth, and therefore they are not transmitted through the ring, thus leading to signal distortion [2]. For the FSRC

modulator [left of Fig. 1(a)], the FSR equals the modulation frequency (f_M), and the generated sidebands are transmitted through the ring; thus the signal is preserved. In order to transmit the sidebands, one needs to excite the spatial modes of the ring resonator at these sideband frequencies. This is achieved by inducing coupling between the resonance mode ω_m at the laser frequency and the adjacent FSR modes ω_{m+1} and ω_{m-1} at the sidebands. In order to induce efficient coupling, we use the method described in [6–8] to break the orthogonality between the adjacent FSR resonance modes by modulating only a portion of the ring ($S < L$, where S is the electrode segment length, and L is the ring circumference) as shown in Fig. 1(b). By assuming the electrode is lumped such that the modulation at the electrode segment is uniform [14], the coupling between two FSR modes with indices m and n can be obtained as

$$\mu_{nm}(t) = -\frac{\omega_n}{4} \int \delta\epsilon(z, t) E_{r,n} E_{r,m}^* dx dy dz, \quad (1)$$

$$\int \frac{1}{2} \epsilon E_{r,m} E_{r,m}^* dx dy dz$$

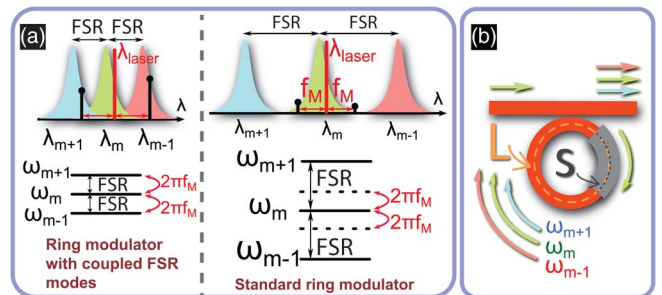


Fig. 1. (a) Depiction of the optical spectra of the FSRC approach (left) and the standard ring modulator (right) under a sinusoidal modulation with frequency f_M . In our FSRC approach, the FSR matches f_M , while in the standard ring modulator, $\text{FSR} \gg f_M$. (b) Illustration of the FSRC scheme. The ring has a circumference, L , and a segment length, S , subjected to refractive index modulation.

where $\omega_n(m)$ and $E_{r,n(m)} = E(x, y)e^{jn(m)2\pi z/L}$ are the resonance angular frequency and the spatial electric field for the $n(m)$ th FSR mode, ϵ is the dielectric constant, $\delta\epsilon(z, t)$ is the dielectric constant modulation, x and y are the cross-sectional axes of the waveguide, and z axis is the direction along the perimeter of the ring. Figure 2(a) shows $|\mu_{nm}|$ calculated from Eq. (1) normalized to the maximum resonance frequency modulation (when $S = L$). The coupling between the nearest adjacent resonances ($|m - n| = 1$) is zero when $S = L$, and it reaches maximum when $S = L/2$. Note that an alternative approach is to use traveling-wave electrodes and modulate the full ring [13], which can provide higher modulation efficiency. However, the challenge in traveling wave electrodes with an integrated pn depletion-type [1] silicon diode is to optimize the RF impedance matching, the velocity matching between the optical and the RF wave, and the RF loss at high RFs [15].

The FSRC modulator is suitable for high RF carrier frequency and narrow-bandwidth analog applications. In Fig. 2(b), we show numerical calculation of the modulation responses (normalized to the response at 1 GHz) for the FSRC modulator (FSR = 26 GHz) and the standard modulator (FSR = 750 GHz) with a different loaded quality factor (Q) when $S = L/4$. Here we calculate the transmission through a ring resonator taking into account of nine adjacent FSR ($m, m \pm 1, m \pm 2, m \pm 3, m \pm 4$) resonance modes using the dynamical equations derived from the coupled mode theory [16]. Note that nine modes are considered because the laser not only couples to the first nearest FSR modes ($m \pm 1$), but also couples to the second (and higher) nearest FSR modes ($m \pm 2, m \pm 3, \dots$) through cascaded coupling. The couplings between these nine resonance modes are determined from Eq. (1). In Fig. 2(b), we see that for $Q = 16,000$, the response for the standard modulator (black) has a sharp roll-off beyond the resonance linewidth, and the response for the FSRC modulator (red) remains relatively flat up to the FSR frequency. In contrast, when the Q is high ($= 60,000$), the modulation response improves but only over a narrow bandwidth at $f_M \approx \text{FSR}$. This indicates that when Q is high, the desired case for lower power consumption, this modulator is inherently narrow-bandwidth, and signal distortion is expected when performing digital data modulation at data rates above the resonance linewidth.

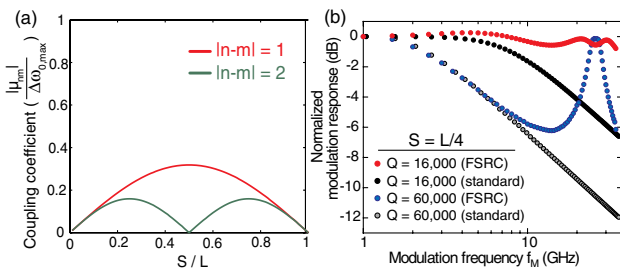


Fig. 2. Calculation of (a) coupling coefficients between two FSR modes with indices m and n normalized to the maximum resonance frequency modulation $\Delta\omega_{0,\max}$ at $S = L$. (b) The modulation responses of the FSRC modulators (colored) and of the standard modulators (black and gray) with $Q = 16,000$ and $Q = 60,000$.

We design and fabricate our silicon ring modulator with an FSR of 26 GHz and compare its performance to a standard ring modulator. The optical microscope image of the device is shown in Fig. 3(a). The radius of the ring is 445 μm , and one quarter of the ring is covered with an electrode. In this quarter region, a p - n diode is also formed inside the silicon waveguide as shown in Fig. 3(b) to provide fast modulation speed in silicon [1]. We chose $S = L/4$ over $L/2$ (higher coupling and modulation efficiency) to prove the concept of the FSRC modulator since this design not only has sufficient coupling [as shown in Figs. 2(a) and 2(b)], but also provides higher electrical bandwidth (lower capacitance). The silicon ring has a cross-sectional dimension of 200 nm \times 450 nm on top of a 50 nm silicon slab. This waveguide dimension supports a single transverse-electric (TE) mode. Note that, although the current modulator is no longer compact, its radius reduces at higher f_M . For example, the radius of the FSRC modulator $\approx 114 \mu\text{m}$ at $f_M = \text{FSR} = 100 \text{ GHz}$, smaller than the size of regular Mach-Zehnder interferometer-based modulator, for example [17]. We also fabricate a standard ring modulator with a radius of 15 μm with a very large FSR of 750 GHz for comparison. The fabrication process is described in [18] (except no heaters are incorporated), and the doping level of the p - and the n -doped regions are $8 \times 10^{17} \text{ 1/cm}^3$, and that of the p^+ - and n^+ -doped regions are $1 \times 10^{20} \text{ 1/cm}^3$.

Our device exhibits an enhancement of the modulation response at 20 GHz larger than the resonance linewidth of 11.7 GHz (calculated from a Q of 16,000). Figure 4 shows the modulation response (normalized to the response at 1 GHz) for both the FSRC modulator (red) and the standard modulator (black). The experiment is performed by applying a small RF signal (-17 dBm) from one port of the network analyzer (NA) to the device pad. The output light is then collected and sent to a high-speed photodiode, which is connected to the other port of the NA, and the scattering matrix element S_{21} is measured. In Fig. 4, the two experimental response curves have similar traces at frequencies up to the resonance linewidth of 11.7 GHz [notice that both the FSRC and the standard modulator have the same Q of 16,000 as shown in the insets of Figs. 5(a) and 5(b)]. However, when $f_M > 11.7 \text{ GHz}$, the response of the standard modulator decreases, with a sharp roll-off as expected, whereas the response of the FSRC modulator increases with a local maximum at 20 GHz. One can see a significant improvement of 8 dB in the response of the FSRC modulator compared to the standard modulator at 27 GHz. Our data in

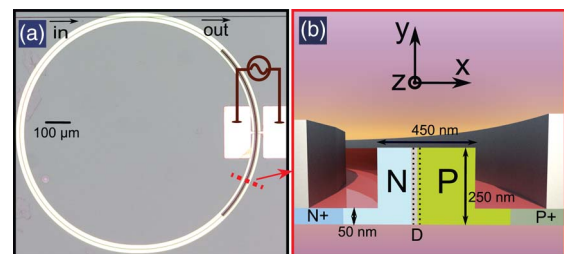


Fig. 3. (a) Optical microscope image of the fabricated device. (b) Illustration of the cross section of the modulated region.

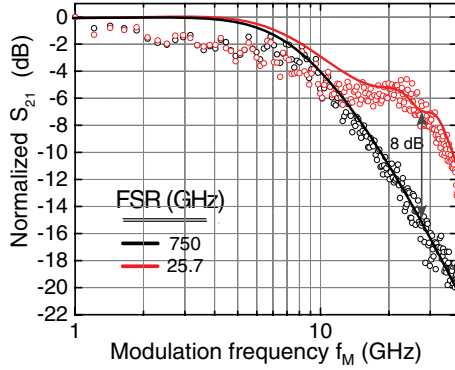


Fig. 4. Measured (circles) and theoretical (solid) modulation responses of the FSRC modulator (red) and the standard modulator (black).

Fig. 4 show steeper roll-offs when compared to the calculation in Fig. 2(b). This is because our fabricated devices are limited by the RC bandwidth. The measured electrical resistance and capacitance for the FSRC (standard) modulator are 11Ω (545Ω) and 190 fF (17 fF), respectively, corresponding to an electrical bandwidth of 14 GHz (16 GHz) in a 50Ω system. In Fig. 4, we also plot the theory curves (solid) that include the RC effects. One can see good agreement between the experiments and the theory curves. The RC effect can be mitigated by further improving the fabrication and optimizing the device structure to lower the resistance and capacitance.

We show that the modulation response enhancement is caused by the coupling between adjacent FSR modes by measuring the optical spectra of our devices under RF modulations. The measurements are done by applying a 5 dBm RF sinusoid signal from a signal generator to the device. The spectra for the FSRC and the standard modulator are shown in Figs. 5(a) and 5(b), respectively. In both figures, the broad peaks in the middle of the spectra are located at the laser wavelength biased on the slope of the resonance curve. The smaller peaks located on the left and the right sides of the broad peaks are the modulation sidebands. In Fig. 5(a), for the FSRC modulator, the sidebands increase as f_M increases, reaching local maxima at $f_M = 20 \text{ GHz}$ (orange) and at 25 GHz (red) on the right and the left side of the broad peak, respectively. For the standard modulator [Fig. 5(b)], the average power of the sidebands drops from -55.17 dBm to -73.15 dBm as f_M increases from 10 to 30 GHz , whereas

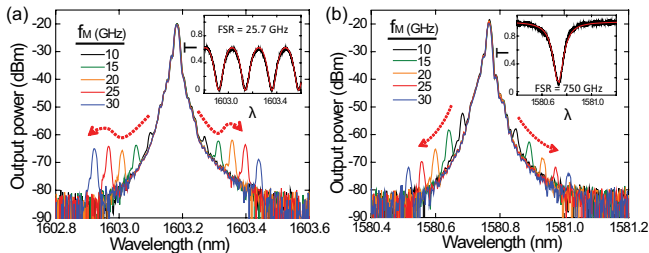


Fig. 5. Optical spectra of the devices modulated with pure sinusoids at different frequencies for (a) the FSRC-coupling modulator and (b) the standard modulator. The insets in (a) and (b) show the measured (black) and the simulated (red) passive optical transmission (T) spectra of the corresponding ring modulators. Both resonators show a loaded quality factor Q of $16,000$.

that of the FSRC modulator decreases less from -59.9 to -66.9 dBm . These results indicate that the sidebands of the FSRC modulator are coupled to the nearest neighboring modes at ± 1 FSR away from the laser wavelength.

For high-modulation frequencies, the FSRC modulator has lower power consumption compared to standard silicon ring modulators. This effect is shown in Fig. 6, where we plot the theoretical power consumption for both the FSRC modulator (red and blue) and the standard silicon ring modulators (black) at different f_M . For this theoretical analysis, the power consumption is calculated from the expression $(1/2)f_M C_d V_d^2$, where C_d is the diode capacitance and V_d is the voltage required to shift the resonance frequency by one resonance linewidth in each cycle of a sinusoid modulation (the laser is on resonance when no voltage is applied). The waveguide and doping geometry adopted for the simulations are shown in Fig. 3(b). The voltage dependence of the carrier distribution and C_d are calculated using SILVACO. These simulated carrier distributions are then imported into COMSOL to calculate the doping-induced loss and the resonance frequency shift to determine Q and V_d , respectively. The standard silicon ring modulator in this analysis has a compact ring radius of $2.5 \mu\text{m}$, a uniform modulation ($S = L$), and a varying Q with the resonance linewidth corresponding to f_M . The FSRC modulator in this analysis has a varying ring radius with an FSR that matches f_M . In all cases, we include a 1 dB/cm scattering loss to account for the fabrication imperfections of the ring [19]. For our proof-of-concept experiment shown in Figs. 3 and 4, where $S = L/4$ and $Q = 16,000$, the power consumption is calculated as $\approx 600 \text{ mW}$. Note that this power can be significantly reduced by designing the modulator with higher Q and f_M . In Fig. 6, we see that when $f_M > 51 \text{ GHz}$, the $S = L/2$ FSRC modulator with a $Q = 80,000$ ($C_d \approx 214 \text{ fF}$ and $V_d \approx 1.6 \text{ V}$) has lower power consumption than that of the standard modulator ($C_d \approx 195 \text{ fF}$ and $V_d \approx 2.3 \text{ V}$). This is true because in standard ring modulator designs, one needs to lower the Q significantly to accommodate higher f_M and because, at higher frequencies, the $\text{FSR} = f_M$ condition is satisfied with smaller rings and hence smaller C_d . Thus the amount of carriers injected and extracted from the depletion region D [see Fig. 3(b)] is reduced. Moreover, as shown in Fig. 6, the modulator with larger electrode ($S = L/2$) consumes less power:

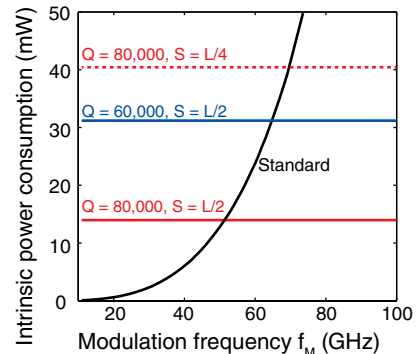


Fig. 6. Theoretical intrinsic power consumptions for the standard silicon ring modulator (black) and the FSRC modulators (colored) with different Q and S .

≈ 14 mW ($Q = 80,000$) versus ≈ 40.5 mW ($Q = 80,000$) for $S = L/4$ electrode because the modulation efficiency increases as the electrode covers a larger portion of the ring. However, when S is large (e.g., $S \geq L/2$) such that the electrode length is comparable to the RF wavelength, the lumped element analysis in Eq. (1) is no longer valid. One possible solution is to further discretize the electrode into smaller segments.

In summary, we have shown high RF carrier frequency modulation of a silicon ring resonator using the coupling between neighboring FSR resonances. The power consumption of FSRC modulators is low at higher f_M because the size of the resonator scales inversely with increasing f_M , and the quality factor can be maintained high (to further decrease the power consumption). This modulator architecture is suitable for high-frequency analog applications using existing CMOS technology. One important parameter for an analog modulator is its linearity and dynamic range. Our preliminary analysis shows that the linearity for the FSRC modulator is similar to that of the standard ring modulator when the signal bandwidth is narrower than the resonance linewidth. When compared to LiNbO₃ [6] and polymer [13] modulators, although silicon ring modulators have lower optical Q and weaker electro-optic effect, they are generally smaller in size because of the higher refractive index resulting in a shorter electrode length. This also leads to lower RF loss and better tolerance of the velocity mismatch for silicon ring modulators with traveling-wave electrodes.

This work was supported by the National Science Foundation through CIAN ERC under grant EEC-0812072 and by the National Science Foundation and Semiconductor Research Corporation under grant ECCS-0903406 SRC Task 2001. This work was also supported by the National Science Foundation under grant no. 1202265. This work was performed in part at the Cornell Nanoscale Facility, a member of the National Nanotechnology Infrastructure Network, which is supported by the National Science Foundation. This work also made use of the Cornell Center for Materials Research Shared Facilities, which are supported through the NSF MRSEC program (DMR-1120296).

References and Notes

1. F. Gardes, G. Reed, N. Emerson, and C. Png, *Opt. Express* **13**, 8845 (2005).
2. P. Dong, R. Shaiha, S. Liao, H. Liang, N.-N. Feng, D. Feng, G. Li, X. Zheng, A. V. Krishnamoorthy, and M. Asghari, *Opt. Express* **18**, 10941 (2010).
3. M. R. Watts, W. A. Zortman, D. C. Trotter, R. W. Young, and A. L. Lentine, *Opt. Express* **19**, 21989 (2011).
4. I.-L. Gheorma and R. Osgood, Jr., *IEEE Photon. Technol. Lett.* **14**, 795 (2002).
5. J. Capmany and D. Novak, *Nat. Photonics* **1**, 319 (2007).
6. D. Cohen, M. Hossein-Zadeh, and A. Levi, *Solid-State Electron.* **45**, 1577 (2001).
7. P. Dong, S. F. Preble, J. T. Robinson, S. Manipatruni, and M. Lipson, *Phys. Rev. Lett.* **100**, 033904 (2008).
8. B. A. Daniel, D. N. Maywar, and G. P. Agrawal, *J. Opt. Soc. Am. B* **28**, 2207 (2011).
9. W. D. Sacher and J. K. Poon, *Opt. Express* **16**, 15741 (2008).
10. W. D. Sacher, W. M. J. Green, S. Assefa, T. Barwicz, H. Pan, S. M. Shank, Y. A. Vlasov, and J. K. S. Poon, *Opt. Express* **21**, 9722 (2013).
11. K. Lau, *Appl. Phys. Lett.* **52**, 2214 (1988).
12. J. B. Georges, M.-H. Kiang, K. Heppell, M. Sayed, and K. Lan, *IEEE Photon. Technol. Lett.* **6**, 568 (1994).
13. B. Bortnik, Y.-C. Hung, H. Tazawa, B.-J. Seo, J. Luo, A. K.-Y. Jen, W. H. Steier, and H. R. Fetterman, *IEEE J. Sel. Top. Quantum Electron.* **13**, 104 (2007).
14. Based on our analysis for the FSRC modulator, the RF wavelength is about eight times of the half electrode length (since the electrode is fed at the midpoint of the electrode) at the FSR frequency considered in this work. Therefore, a lumped model is a valid approximation.
15. H. Yu and W. Bogaerts, *J. Lightwave Technol.* **30**, 1602 (2012).
16. H. A. Haus and W. Huang, *Proc. IEEE* **79**, 1505 (1991).
17. D. J. Thomson, F. Y. Gardes, J.-M. Fedeli, S. Zlatanovic, Y. Hu, B. P. P. Kuo, E. Myslivets, N. Alic, S. Radic, G. Z. Mashanovich, and G. T. Reed, *IEEE Photon. Technol. Lett.* **24**, 234 (2012).
18. J. Cardenas, P. A. Morton, J. B. Khurgin, A. Grith, C. B. Poitras, K. Preston, and M. Lipson, *Opt. Express* **21**, 22549 (2013).
19. A. Grith, J. Cardenas, C. B. Poitras, and M. Lipson, *Opt. Express* **20**, 21341 (2012).